Development/Plasticity/Repair

# The Relationship between PSD-95 Clustering and Spine Stability *In Vivo*

**Michele Cane,[1,2] Bohumil Maco,[3,4] Graham Knott,[3] and Anthony Holtmaat[1]**

[1]Department of Basic Neurosciences, Faculty of Medicine and the Geneva Neuroscience Center, University of Geneva, CH 1211, Switzerland, and [2]Lemanic Neuroscience Doctoral School, [3]Biological Electron Microscopy Facility, Centre of Electron Microscopy, and [4]Computer Vision Laboratory, École Polytechnique Fédérale de Lausanne, Lausanne, CH 1015, Switzerland

**The appearance and disappearance of dendritic spines, accompanied by synapse formation and elimination may underlie the experience-dependent reorganization of cortical circuits. The exact temporal relationship between spine and synapse formation *in vivo* remains unclear, as does the extent to which synapse formation enhances the stability of newly formed spines and whether transient spines produce synapses. We used *in utero* electroporation of DsRedExpress- and eGFP-tagged postsynaptic density protein 95 (PSD-95) to investigate the relationship between spine and PSD stability in mouse neocortical L2/3 pyramidal cells *in vivo*. Similar to previous studies, spines and synapses appeared and disappeared, even in naive animals. Cytosolic spine volumes and PSD-95-eGFP levels in spines covaried over time, suggesting that the strength of many individual synapses continuously changes in the adult neocortex. The minority of newly formed spines acquired PSD-95-eGFP puncta. Spines that failed to acquire a PSD rarely survived for more than a day. Although PSD-95-eGFP accumulation was associated with increased spine lifetimes, most new spines with a PSD did not convert into persistent spines. This indicates that transient spines may serve to produce short-lived synaptic contacts. Persistent spines that were destined to disappear showed, on average, reduced PSD-95-eGFP levels well before the actual pruning event. Altogether, our data indicate that the PSD size relates to spine stability *in vivo*.**

## Introduction

The formation of new synapses at the expense of old synapses may underlie the experience-dependent and functional reorganization of cortical circuits in adults (Holtmaat and Svoboda, 2009; Fu and Zuo, 2011). Imaging studies *in vivo* have shown that proxies for synapses, such as dendritic spines and axonal boutons, appear and disappear over days, even in naive mice. Under baseline conditions, new dendritic spines rarely transform into persistent spines and usually retract within hours and days after they are formed (Holtmaat et al., 2005; Zuo et al., 2005). These transient spines were hypothesized to generate short-lived synaptic contacts. Indeed, *in vitro* studies have shown that new spines can display transmitter-evoked $Ca^{2+}$ transients within hours (Zito et al., 2009) and often rapidly incorporate morphologically mature synapses (Nägerl et al., 2007; Zito et al., 2009). However, retrospective electron microscopy (EM) on dendrites that were imaged *in vivo* has shown that a large fraction of new spines do not bear a morphologically defined synapse within the first day (Knott et al., 2006); but they always contain synapses after several days and their sizes correlate with the spines' lifetimes. This suggests that synapse growth *in vivo* is slow and that spine stabilization and synapse growth are closely linked. It also implies that transient spines are new spines that fail to form a synapse. However, because the findings were based on end-point measurements, it remains uncertain whether synapse formation *in vivo* is a unique signature of new persistent spines. Neither do we know whether new spine survival and pruning *in vivo* is associated with synapse growth or shrinkage, respectively.

To answer these questions, we expressed PSD-95-eGFP in adult L2/3 pyramidal cells of the barrel cortex using *in utero* electroporation and imaged dendritic spines *in vivo*. PSD-95 is a postsynaptic scaffold protein that is present in the majority of excitatory synapses and interlinks a variety of proteins (Craven et al., 1999; Chen et al., 2005; Sheng and Hoogenraad, 2007). PSD-95 modulates postsynaptic function and maturation (El-Husseini et al., 2000; Ehrlich et al., 2007). Expression of PSD-95-eGFP allows the visualization of postsynaptic densities (PSDs) in real time *in vitro* (Okabe et al., 1999; Sala et al., 2003; Sharma et al., 2006; Woods et al., 2011) and *in vivo* (Niell et al., 2004; Gray et al., 2006; Kelsch et al., 2008; Livneh et al., 2009) without disturbing gross synaptic network dynamics (Gray et al., 2006). Such experiments have indicated that the appearance and disappearance of fluorescently labeled PSD-95 puncta is likely to represent

Received Aug. 6, 2013; revised Nov. 21, 2013; accepted Dec. 20, 2013.

Author contributions: M.C., G.K., and A.H. designed research; M.C., B.M., G.K., and A.H. performed research; M.C., B.M., G.K., and A.H. analyzed data; M.C. and A.H. wrote the paper.

This work was supported by the Swiss National Science Foundation (Grants 31003A_120685 (AH), 31003A_135631 (AH), CRSI33_127289 (AH), and CRFII313470/1 to G.K.); the International Foundation for Research in Paraplegia; and the Hans Wilsdorf Foundation (Dr Alain Rossier Chair funding to A.H.). We thank Simon Borgeaud, Laurant Brodier, and Alberto Bisco for help with image analysis; Daniel Lebrecht and Aurelie Pala for advise on single-cell electroporation experiments; Marco Cantoni for help with the FIBSEM imaging; Michael Patterson and Stéphane Pagès for comments on our manuscript; Roby Weimer, Noah Gray, and Karel Svoboda for initial help with the experiments and for sharing the PSD-95-eGFP and DsRedExpress plasmids; and Karel Svoboda, Sen Song, Vijay Iyer, and Tim O'Connor for sharing image analysis software.

The authors declare no competing financial interests.

Correspondence should be addressed to Anthony Holtmaat, Department of Basic Neurosciences, CMU, 1 rue Michel Servet, 1211 Geneva-4, Switzerland. E-mail: anthony.holtmaat@unige.ch.

DOI:10.1523/JNEUROSCI.3353-13.2014

Copyright © 2014 the authors 0270-6474/14/342075-12$15.00/0

synapse formation and synaptic pruning (Prange and Murphy, 2001; De Roo et al., 2008; Chen et al., 2011).

Our data confirm that PSDs are dynamic *in vivo* and imply that spine maintenance is associated with the presence of a PSD and may even depend on its size. The accumulation of PSD-95 is associated with (new) spine survival. However, the presence of a PSD is not an exclusive attribute of persistent spines; a small fraction of transient spines may serve to produce short-lived synaptic contacts.

## Materials and Methods

### *DNA constructs*

The pCAG-PSD-95-eGFP-WPRE and pCAG-DsRedExpress-WPRE plasmids were obtained from K. Svoboda, Janelia Research Farms (Gray et al., 2006). In the PSD-95-eGFP plasmid, the eGFP open reading frame was placed in frame at the 3′ translated region of PSD-95, which codes for the c-terminal part of the PSD-95 protein (Okabe et al., 1999). In both plasmids, expression was driven by the CMV-enhanced chicken $\beta$-actin promoter (CAG). The 3′ untranslated regions contained the woodchuck hepatitis virus posttranslational regulatory element (WPRE) and the bovine growth hormone polyadenylation site.

### *Electroporation*

This study was performed according to the guidelines of the Swiss Federal Act on Animal Protection and Swiss Animal Protection Ordinance. All experiments were approved by the ethics committee of the University of Geneva and the Cantonal Veterinary Office (Geneva, Switzerland).

*In utero* electroporations were performed as described previously (Saito and Nakatsuji, 2001; Tabata and Nakajima, 2001; Fig. 1*A*). In short, E16 timed-pregnant C57BL/6J mice were anesthetized using an isoflurane–oxygen mixture (2% vol isoflurane/vol $O_2$). The uterine horns were exposed through a ~1 cm incision on the abdominal wall. Approximately 1 $\mu$l of buffer solution containing ~2 $\mu$g/$\mu$l pCAG-PSD-95-eGFP-WPRE plasmid, a molar equivalent of pCAG-DsRedExpress-WPRE plasmid, and a trace of Fast Green (Sigma) was injected using a custom-made intracellular microinjection dispense system that was controlled by a pulse stimulator (Master-8; A.M.P.I.). The fluid was injected into the right lateral ventricle of each embryo through a pulled-glass pipette. Subsequently, the head of each embryo was placed between custom-made tweezer electrodes with the positive electrode contacting the right side of the head. Electroporation into the right cerebral cortex was achieved using 5 square pulses (duration = 50 ms, frequency = 1 Hz, 40 V).

The single cell electroporation was performed as described previously (Judkewitz et al., 2009). The procedure was performed on a 6-week-old C57BL/6 male. An intracellular solution containing ~100 ng/$\mu$l pCAG-PSD-95-eGFP-WPRE plasmid and a molar equivalent of pCAG-DsRedExpress-WPRE plasmid was used.

### *Cranial window*

At postnatal day 42, mice were anesthetized with a ketamine (0.10 mg/g body weight) and xylazine (0.01 mg/g body weight) mixture. The cranial windows were implanted as described previously (Holtmaat et al., 2009; Fig. 1*B*). Before the surgery, dexamethasone (~2 $\mu$g/g body weight) was injected intramuscularly to reduce cerebral edema during the craniotomy. The craniotomy was located above the right somatosensory cortex (~1.5 mm caudal and ~3 mm lateral of bregma). The craniotomy was covered with a 5-mm-diameter cover glass, which was permanently glued to the skull using dental acrylic cement. The dura remained intact. After surgery, the animals received buprenorphine (0.1 $\mu$g/g body weight, s.c.) and carprofen (5 $\mu$g/g body weight, i.p.) to reduce pain and inflammation. Imaging was started 2 weeks after cranial window implantation.

### *Imaging*

*In vivo* images were acquired under isoflurane anesthesia (1% vol isoflurane/vol $O_2$) using a custom-built, two-photon laser-scanning microscope (2PLSM; Holtmaat et al., 2009) controlled by custom software written in MATLAB (Scanimage; Janelia Research Farm; Pologruto et al., 2003). As a light source, we used a tunable Ti:sapphire laser (Chameleon ultra II; Coherent) running at 940 nm for simultaneous excitation of eGFP and DsRedExpress (typically 80–120 mW at the back focal plane of the objective). The microscope was equipped with a 40×, 0.8 numerical aperture water-immersion objective (Olympus) and high-quantum-efficiency photomultiplier tubes (R3896; Hamamatsu). Emitted light was spectrally separated using a 565 nm dichroic mirror (Chroma) and two band-pass filters (510/50 nm and 620/60 nm; Chroma). Typically, the mice coexpressed PSD-95-eGFP and DsRedExpress in a large subset of L2/3 pyramidal cells under the cranial window (Fig. 1*B*,*C*). Dendrites were imaged for 2 weeks over various time intervals (6, 18, and 96 h; Fig. 1*D*). Images were acquired at 2 ms/line (image size, 512 × 512 pixels; pixel size, 0.06 × 0.06 $\mu$m).

### *Focused ion beam scanning electron microscopy*

EM of an *in vivo* imaged dendrite was performed using the same method as described previously (Maco et al., 2013). The mouse was perfused via the heart immediately after the live imaging using a buffered mix of 2% paraformaldehyde and 2.5% glutaraldehyde in PB (0.1 M, pH 7.4). Two hours later, the brain was removed and 60-$\mu$m-thick Vibratome sections cut tangentially to the imaged region. The section containing the dendrites of interest was then imaged again in the two-photon microscope. Using the laser, fiducial marks were burnt into the fixed tissue around the portion of dendrite required for EM analysis.

The section was then washed in cacodylate buffer (0.1 M, pH 7.4) and postfixed and stained in 1.5% potassium ferrocyanide with 1% osmium tetroxide, followed by 1% osmium tetroxide alone and then finally 1% aqueous uranyl acetate. Sections were dehydrated in graded alcohol series and embedded in Durcupan resin.

Once the resin had hardened, the region containing the laser marks was mounted onto a flat, blank resin slab and trimmed with a glass knife and ultramicrotome ready for the electron microscope. The portion of the block containing the fiducial marks was imaged inside an NVision 40 FIBSEM microscope (Carl Zeiss) using an acceleration voltage of 1.5 kV, current of 350 pA, and dwell time of 10 $\mu$s/pixel. The images were collected at a magnification of 6 nm/pixel. The milling depth between images was 12 nm. The entire image series was aligned in the Fiji software (http://fiji.sc/wiki/index.php/Fiji) and the dendrites of interest manually segmented using TrakEM2 program in Fiji software (Cardona et al., 2012). The Blender software (www.blender.org) was used for the final visualization and measurements of the synaptic surface areas.

### *Image analysis*

*Scoring of spines and PSD-95-eGFP-puncta.* A custom-written MATLAB program (Holtmaat et al., 2009) was used to analyze dendritic spines and PSD-95 puncta dynamics in three dimensions over the 13 imaging sessions. We collected data from 7 C57BL/6J mice (6 males and 1 female), including 1583 spines or PSD-95 puncta (a total number of ~10,000 spines or puncta were detected over the whole time course of the experiment, including gained and lost elements), with the number of structures per animal ranging from 122 to 480. Only spines that were emanating laterally from dendritic shaft were included. Protrusions or PSD-95 puncta were scored manually using strict criteria. To assess rapidly during the scoring procedure whether a spine contained a PSD-95-eGFP punctum, a region smaller than the spine head was selected in the green channel ($Sp_G$; Fig. 2*B*, gray arrowhead). Several (3–4) regions of the same size were selected in the dendritic shaft just below the spine (Fig. 2*B*, black arrowhead), carefully avoiding unambiguous PSD-95-eGFP concentrations ($D_G$; Fig. 2*B*, open arrowhead), and averaged. Presumptive PSD-95 puncta within the shaft were analyzed similarly. We denoted a punctum if the intensity of $Sp_G$ was 10% brighter than the average of $D_G$ and 5× higher than the SD of this average. This analysis revealed three different groups: spines with a PSD-95-eGFP punctum, spines without a PSD-95-eGFP punctum, and PSD-95-eGFP puncta without a discernible spine. In a subset of spines ($n$ = 217), we measured the fraction of diffusible PSD-95-eGFP that was bound in the spine head using a method described previously (Otmakhov et al., 2004). The fluorescence intensities were taken the same regions as described above, including both channels ($[Sp_G - D_G \cdot \{Sp_R/D_R\}]/Sp_G$). Background pixel values were sub-

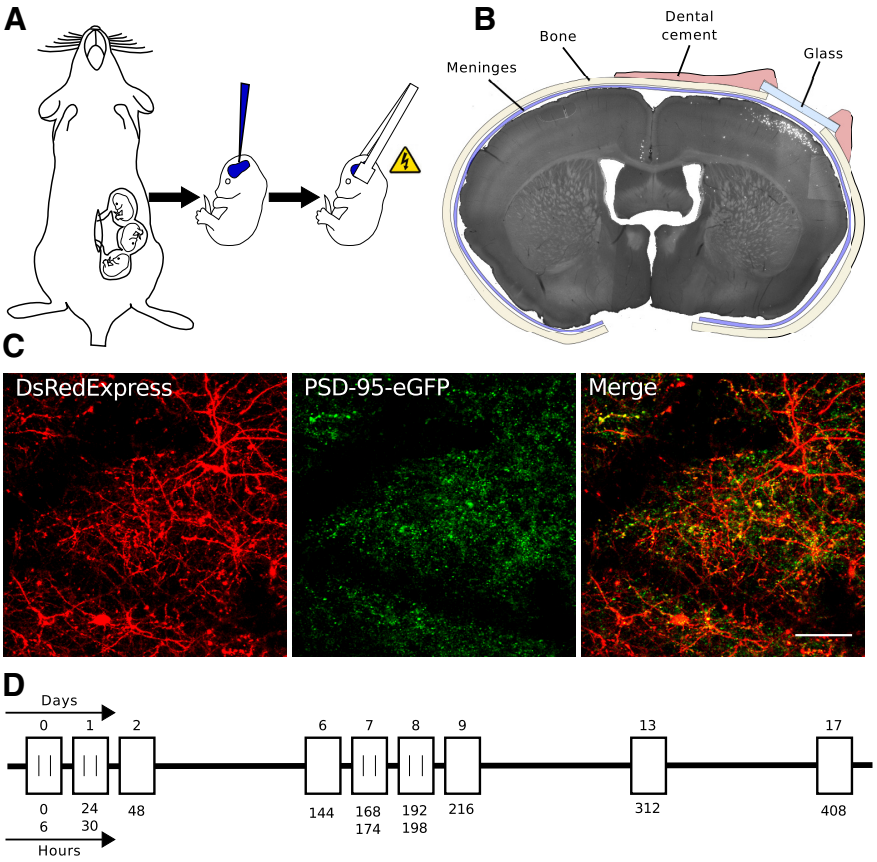


**Figure 1.** ***A***, Mixture of CAG-PSD-95-eGFP-WPRE and CAG-DsRedExpress-WPRE plasmids was injected in the lateral cerebral ventricle of E16 embryos *in utero*. Neurons were electroporated using electrode tweezers. ***B***, Coronal section showing a large group of labeled L2/3 pyramidal cells in the barrel cortex located under the craniotomy. ***C***, *In vivo* 2PLSM image of the transfected area (scale bar, 50 $\mu$m), showing a partial colocalization of the two fluorescent proteins. ***D***, Timeline of the imaging sessions. Boxes indicate days, ticks indicate multiple imaging sessions per day.

tracted. Negative accumulation values and values >1 were set to 0 because these were caused by near-background pixel intensities. We used a two-partioning *k*-means cluster analysis (MATLAB) to separate the presumptive SpO and SpP populations. This method produced nearly similar results (Fig. 2*C*).

*Quantification of fluorescence intensities.* 2PLSM and retrospective EM showed that spine volumes are proportional to spine brightness (Holtmaat et al., 2005). Therefore, we used relative DsRedExpress and eGFP brightness in single two-photon optical sections to estimate relative spine volumes and PSD sizes, respectively (Fig. 5*B*). Spine fluorescence was calculated by integrating the pixel values of a selected area around the spine head of the brightest section (Fig. 5*B*, circle). An average background pixel value was calculated from an area on the same section next to the spine (Fig. 5*B*, box). The background pixel value was subtracted from each pixel of the spine area. Because dendritic shaft diameters were constant and relatively uniform, we used them to correct the spine fluorescence levels for possible variations in excitation and detection efficiencies. For each spine, we selected a region (1–3 $\mu$m long) in the dendritic shaft. The average of the background-subtracted brightest pixels along this specified region was calculated using custom software written in MATLAB (kindly provided by Sen Song; Grillo et al., 2013) and used as a normalization factor. The spine and PSD-95-eGFP values were expressed as the background-subtracted spine and PSD-95-eGFP intensity divided by the normalization factor. Although this analysis method proved sound for spines on big dendrites (Holtmaat et al., 2005), regions of interest in which the dendrite was very small could occasionally cause extreme spine brightness values. In general, we assumed that the dendritic volume exceeds the point-spread function of the microscope and that the maximum pixel values in the dendrite are linearly related to fluorescent protein expression levels. However, in some cases, dendritic volumes were smaller than the point-spread function and presumably smaller than large spine heads. In these cases, the maximum pixel values in the dendrite did not accurately relate to expression levels, which resulted in an overestimation of the relative spine volume. Similar errors occurred in the green channel. To minimize the influence of these outliers in the regression analysis, we applied a robust least-square regression analysis (MATLAB).

*Spine and PSD size changes over time.* Relative spine and PSD size changes were expressed as the common logarithm ratio of the relative spine brightness on time point 2 over time point 1. Persistent spines were often sampled several times. To estimate the sampling error and the error due to movement noise, we imaged 10 spines on various dendrites 10 times (with 1 min intervals), assuming that spine volume fluctuations are minimal over this time span. The $\log_{10}$ ratio between the highest and lowest value measured over this 10 min period was 0.1.

### *Statistics*

For structure identity analysis, we pooled the spines of all animals and performed binary data statistics ($\chi^2$ test) or paired *t* tests to compare values over animals. For the regression analysis of new spines volumes, we used a robust fitting method (MATLAB). Comparison of fluorescence distributions was performed using a Kolmogorov–Smirnov test. Significance of volume changes was calculated using *t* tests.

## Results

### PSD-95-eGFP expression allows the identification of PSDs

Adult mice that were transfected at embryonic day 16 expressed PSD-95-eGFP and DsRedExpress in L2/3 cortical pyramidal cells (Fig. 1*B*,*C*). We observed coexpression in a large subset of neurons. Neurons that were sufficiently bright in both channels were selected for long-term imaging (2 weeks) of high-magnification regions of interest. (Fig. 1*D*). The linear spine densities ($0.34 \pm 0.02\ \mu m^{-1}$, $n = 39$ dendrites) and spine turnover (22% over 4 d) were similar to previous observations (Holtmaat et al., 2005; Gray et al., 2006). We observed concentrations of PSD-95-eGFP in spines and dendritic shafts (Fig. 2*A*). Such puncta have been shown to represent postsynaptic densities (Okabe et al., 1999; Okabe et al., 2001; Gray et al., 2006). To reproducibly discriminate between putative synaptic and nonsynaptic PSD-95-eGFP concentrations, we measured the ratio of eGFP fluorescence intensities per pixel in a presumptive PSD-95-eGFP punctum and the pixel intensity average of a neighboring region in the dendritic shaft, avoiding clear puncta in the shaft (Fig. 2*B*). We assumed that the dendritic shaft average represents the level of freely diffusing and unbound PSD-95-eGFP (Gray et al., 2006). We arbitrarily defined a PSD-95-eGFP punctum to represent a PSD if its fluorescence intensity was 10% higher than the average in the dendritic shaft and 5× higher than the SD of this average. This threshold resulted in three different types of structures (Fig. 2*A*): (1) protrusions without a PSD-95-eGFP punctum, which we termed "spines only" (SpO; Fig. 2*A*, #1); (2) protrusions with a PSD-95-eGFP punctum, termed

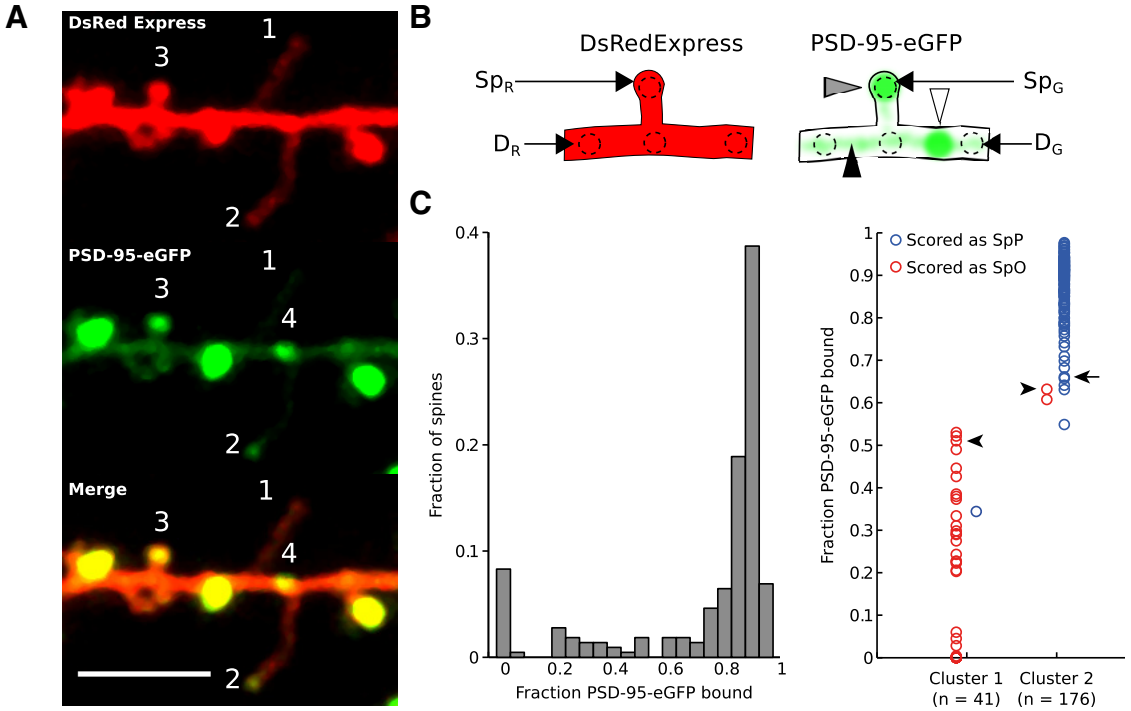


**Figure 2.** ***A***, Dendritic branch imaged at high magnification (scale bar, 5 $\mu$m). Three types of structure are visible: #1, a long thin spine without a PSD-95-eGFP punctum (SpO); #2, a long thin spine with a PSD-95-GFP punctum (SpP); #3, a mushroom-like spine with a PSD-95-eGFP punctum (SpP); and #4, a PSD-95-eGFP punctum in the dendritic shaft (PO). For the sake of visualization, both channels are presented with different lookup tables. ***B***, Procedure to determine the presence of PSD-95-eGFP puncta. PSD-95-eGFP fluorescence (right) in the spine head (gray arrowhead) was determined by integrating pixel values over an area smaller than the spine head ($Sp_G$). This value was divided by the average of the integrated pixel values of several (3–4) equally sized areas ($D_G$) in the dendritic shaft (black arrowhead), carefully avoiding apparent PSD-95-eGFP puncta (open arrowhead) in the shaft. ***C***, Left, Distribution of the fraction of PSD-95-eGFP bound in spine heads ($n = 217$) as measured according to Otmakhov et al. (2004). Right, Result of a *k*-means cluster analysis ($k = 2$) of the spine population from the left graph. Rapid puncta-based scoring results shown in color. Note that our scoring results nearly match the clustering. Arrowheads, two SpOs from Figure 3; arrow, smallest SpP from Figure 3.

"spines with PSD" (SpP; Fig. 2*A*, #2 and #3); and (3) puncta in the dendritic shaft, termed "PSD only" (PO; Fig. 2*A*, #4). It should be noted that the latter structures may represent shaft synapses and synapses on spines that could not be resolved along the optical axis of the microscope. At the start of the experiment, 17.4% of all structures were classified as SpO, 62.5% as SpP, and 20.1% as PO (total $n = 690$ structures; Fig. 4*A*,*B*).

To determine whether this method reliably distinguishes the different classes, we also measured the fraction of bound PSD-95-eGFP in 217 randomly selected spines using a method used previously to index the accumulation of synaptic proteins (Otmakhov et al., 2004). In the majority of spines (76%), the fraction of PSD-95-eGFP bound within the spine head equaled 0.75 or higher. The distribution of bound PSD-95-eGFP fractions displayed a local minimum of ~0.55, suggesting that the spines with and without PSDs may separate around this value (Fig. 2*C*, left). Indeed, a partitioning of the data in 2 clusters (*k*-means cluster analysis) revealed a similar separation value (centroids: cluster 1, fraction bound 0.19 ± 0.19, $n = 41$, and cluster 2, fraction bound 0.88 ± 0.08, $n = 176$), which nearly matched the SpO ($n = 40$) and SpP ($n = 177$) scores, respectively (Fig. 2*C*, right). One SpP fell into cluster 1 and two SpOs fell into cluster 2. The ambiguity in some of the spines (~5% of the SpOs) was probably due to the variability in the PSD-95-GFP and dsRedExpress levels in different dendrites, which was used to normalize spine fluorescence. Therefore, the rapid puncta detection may cause a slight overrepresention of the number of SpOs. Nonetheless, the results suggest that *in vivo* PSD punctum detection methods distinguish the vast majority of PSD-containing spines from the PSD-less structures.

To further investigate the accuracy of the scoring criteria, we used single-cell electroporation of PSD-95-eGFP combined with focused ion beam scanning electron microscopy (FIBSEM; Maco et al., 2013) to reconstruct a dendritic branch of an imaged PSD-95-GFP-expressing neuron that had PSD-95-eGFP-less protrusions (Fig. 3*A*,*E*, #5 and #6) and small PSD-95-eGFP puncta just above the detection threshold (Fig. 3*A*,*E*, #4). All protrusions that were seen in the 2PLSM image were found in the EM reconstruction (compare Fig. 3*A*,*B*), even thin spines with necks thinner than 85 nm (Fig. 3*A*,*B*, #5 and #6). Similarly, all PSD-95-eGFP clusters that we had defined as puncta represented postsynaptic densities in the electron micrographs (Fig. 3*B*–*D*), with the smallest PSD-95-eGFP punctum being among the smallest PSDs that can be observed in FIBSEM. The three protrusions that we had defined as SpOs did not contain a visible postsynaptic density in the EM. The brightness of the puncta displayed a linear relationship with the size of the PSDs, as measured in the EM reconstruction (Fig. 3*C*). This indicates that, *in vivo*, 2PLSM of PSD-95-eGFP reliably detects the smallest PSDs.

### PSD-95-eGFP puncta appear and disappear

Time-lapse imaging revealed many protrusions and PSD-95-eGFP puncta that were present over the whole experiment ($n = 302$). However, as expected and similar to previous *in vivo* imaging studies, some structures appeared or disappeared during the imaging period. A total of 1–5% of the structures that were present from the start until the end were classified as SpOs (1.7% at 0 h, 5.0% at d17; Fig. 4*A*,*B*), whereas 78–82% were SpPs (81.8% at 0 h, 78.4% at d17) and 16% were POs (16.6% at 0 h, 16.6% at d17). This indicates that persistent spines nearly always contain a

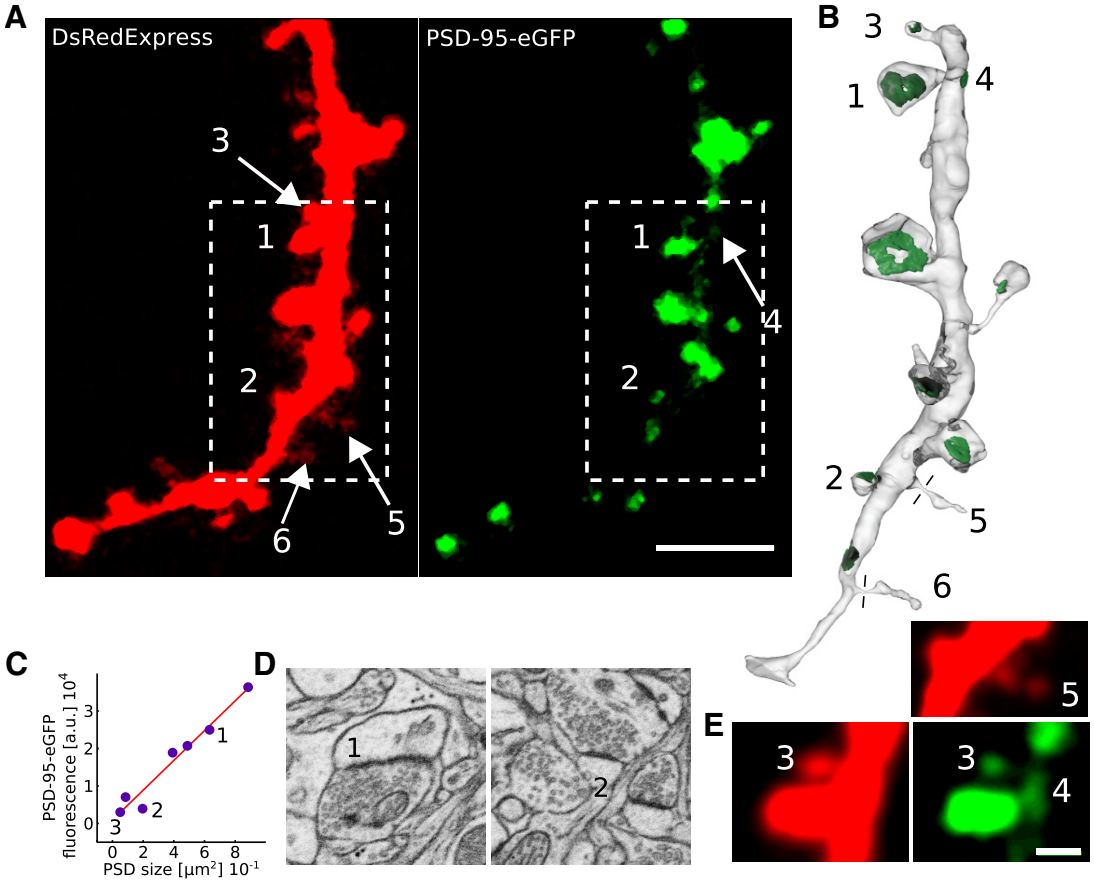


**Figure 3.** ***A***, Dendritic branch of a neuron that was electroporated using a patch pipette in the adult cortex. Left, dsRedExpress. Right, PSD-95-eGFP (scale bar, 5 $\mu$m) ***B***, FIBSEM reconstruction of the boxed region of the dendrite in ***A***. All spines and PSDs match; #1, big mushroom SpP; #2, small mushroom SpP; #3, SpP with the smallest PSD in the reconstruction; #4, PSD on the shaft (PO); #5 and #6, thin spines without PSDs (SpOs). ***C***, Relationship between the size of the PSDs in the EM reconstruction and the normalized fluorescence intensities of PSD-95-eGFP *in vivo*. ***D***, FIBSEM micrographs of two spines (#1 and #2). ***E***, High magnifications of structures #3, #4, and #5 in the red and green channel (images are filtered several times for optimal visualization; scale bar, 1 $\mu$m).

PSD, confirming EM observations (Knott et al., 2006). The majority of structures that were gained and/or lost comprised SpOs at the moment they were observed for the first and last time, respectively (gains: 55.0% SpO, 27.2% SpP, 17.8% PO; losses: 50.5% SpO, 30.9% SpP, 18.6% PO). This indicates that a large fraction of spines that were newly formed did not immediately contain a PSD, confirming previous EM observations (Knott et al., 2006). Similarly, spines that were destined to be lost often did not contain a PSD shortly before they were pruned. However, it should be noted that a large fraction of gained and lost spines comprised transient spines that appeared and disappeared within the time frame of our experiment.

Because synapse formation may be considerably delayed compared with the formation of a dendritic spine (Knott et al., 2006), we calculated the fraction of new and lost spines with a defined PSD for various intervals (6, 18, and 96 h) over which we first or last observed them (Fig. 4*C*,*D*). It should be noted that, here too, both populations contained transient spines. A total of 18.6% of the new spines that appeared over imaging intervals of 6 h contained a PSD. A significantly larger fraction (42.4%, $p < 0.005$, $\chi^2$) of spines first seen over 96 h intervals contained PSDs. This suggests that although synapse formation may happen within hours after the growth of a protrusion, in some protrusions, the accumulation of detectable PSD-95-GFP puncta may take much longer. Similarly, a significantly larger fraction of spines that were last seen before a 96 h imaging interval contained a PSD than before a 6 h interval (96 h, 48.4%; 6 h, 19.4%, $p < 0.005$, $\chi^2$). This suggests that spines destined to disappear gradually lose their PSD over the course of days. Nonetheless, some spines contain a PSD shortly (hours) before they are pruned, in accordance with recent *in vitro* data (Woods et al., 2011).

### Relationship between PSD-95-eGFP clustering and spine stability

Throughout the imaging period, we observed various combinations of spine and PSD stabilities. Persistent spines always bore a PSD (Fig. 5*A*, #1). Many large PSD-95-eGFP puncta in spines were maintained over long time frames, but occasionally they were abruptly lost (Fig. 5*A*, #1) or gradually lost (Fig. 5*H*, #5). Many new spines failed to acquire a clear PSD-95-eGFP punctum on one of our imaging time points and were lost shortly after they were generated (Fig. 5*A*, #3). Some new spines that stabilized incorporated a distinct PSD-95-eGFP punctum (Fig. 5*A*, #4). Occasionally, we saw new spines at least twice without a PSD-95-eGFP punctum (Fig. 5*G*, #6). To investigate quantitatively the relationship between PSD-95 clustering and spine stability, we analyzed the fractions of new spines that accumulated PSD-95-eGFP and compared this with their survival rate (Fig. 5*B*,*C*). First, we measured the fraction of new spines with and without PSDs immediately after they were formed and reassessed this fraction 24 h later (Fig. 5*B*). We analyzed a subset of 193 new spines that were detected on time point $t = 24$ h, $t = 168$ h, or $t =$

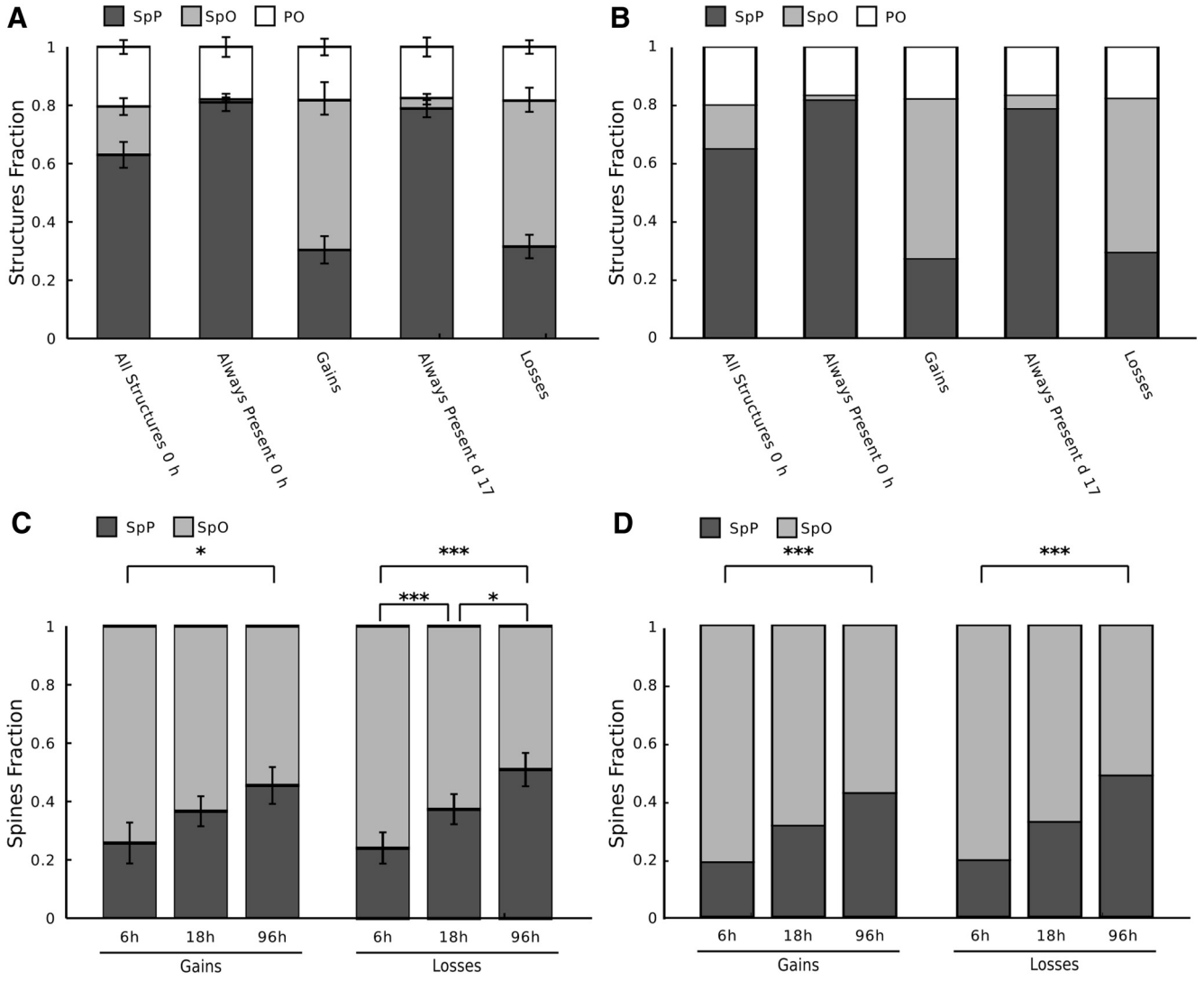


**Figure 4.** ***A***, ***D***, Fraction of spines with a PSD-95-eGFP punctum (SpP, dark gray), spines without a PSD-95-eGFP punctum (SpO, light gray), and PSD-95-eGFP puncta in the dendritic shaft (PO, white). ***C***, ***D***, Fraction of new spines with a PSD-95-eGFP punctum (SpP, dark gray) and new spines without a PSD-95-eGFP punctum (SpO, light gray) for spines appearing over 6, 18, and 96 h intervals (left) and spines disappearing over 6, 18, and 96 h intervals (right). ***A***, ***C***, Averages over mice (*$p < 0.05$; ***$p < 0.005$; paired *t* test). ***B***, ***D***, Structures from all mice pooled (***$p < 0.005$, $\chi^2$).

192 h and did not exist 24 h before these points ($t = 0$ h, 144 h, and 168 h, respectively). A total of 70.5% (136) of spines were devoid of a detectable PSD-95-eGFP punctum. Out of this pool of spines, 17.6% (24 spines) were still present after 24 h. In this subset of new spines, none had accumulated PSD-95-eGFP (but see Fig. 5*A*, spine #4, for an example of a new spine with a delayed acquisition of a PSD). Conversely, 29.5% (57 spines) of the new spines contained a PSD-95-GFP punctum and 59.6% (34) of those were detected again 24 h later. All had maintained their synapses. As a result, the fraction of new spines with a PSD had significantly increased over 24 h (59% at $t = 24$ h, 30% at $t = 0$ h, $p < 0.005$, $\chi^2$). When we tracked new spines that were only up to 6 h old ($n = 161$; Fig. 5*C*), we found that an even smaller fraction contained a PSD-95-eGFP punctum (18.6%, $n = 30$), of which only a small portion survived over the next 18 h (33.3%, $n = 10$). A total of 14.5% of spines that did not contain a PSD-95-eGFP punctum survived over the next 18 h ($n = 19$); 31.6% of these ($n = 6$) had incorporated a PSD. Therefore, of all of the new SpPs that were observed at the second time point ($n = 16$), 37.5% had incorporated PSD over the 18 h interval. This indicates that PSD-95-eGFP accumulation in a new spine is not always immediate and may occur with a delay of >6 h. To assess the relationship between the presence of PSD-95-eGFP and spine survival over longer time frames, we grouped new spines that were seen in at least two imaging sessions into two categories: those that were seen over an interval <96 h (transient spines; Holtmaat et al., 2005) and those with a lifespan of >96 h (Fig. 5*D*). Out of the total number of new spines (721) that had appeared during the experiment, the majority was seen only once (71.1%); 126 (24.6%) of these spines had a PSD when they were detected. A small fraction of the new spines survived for >96 h (14.0%) and the majority of those displayed a PSD at least once (83.2%; 84 of 101). Of the remaining spines (14.9%; i.e., those that were seen at least twice but survived for <96 h), a significantly lower fraction (64.5%; 69 of 107; $p < 0.005$, $\chi^2$) had displayed a PSD punctum at least once. This shows that the presence of a PSD indicates a higher probability for a new spine to stabilize. However, the acquisition of a PSD does not per se predict the stabilization of a spine. In fact, the majority of new spines bearing a PSD at least once disappear before they are 4 d old (69.9%).

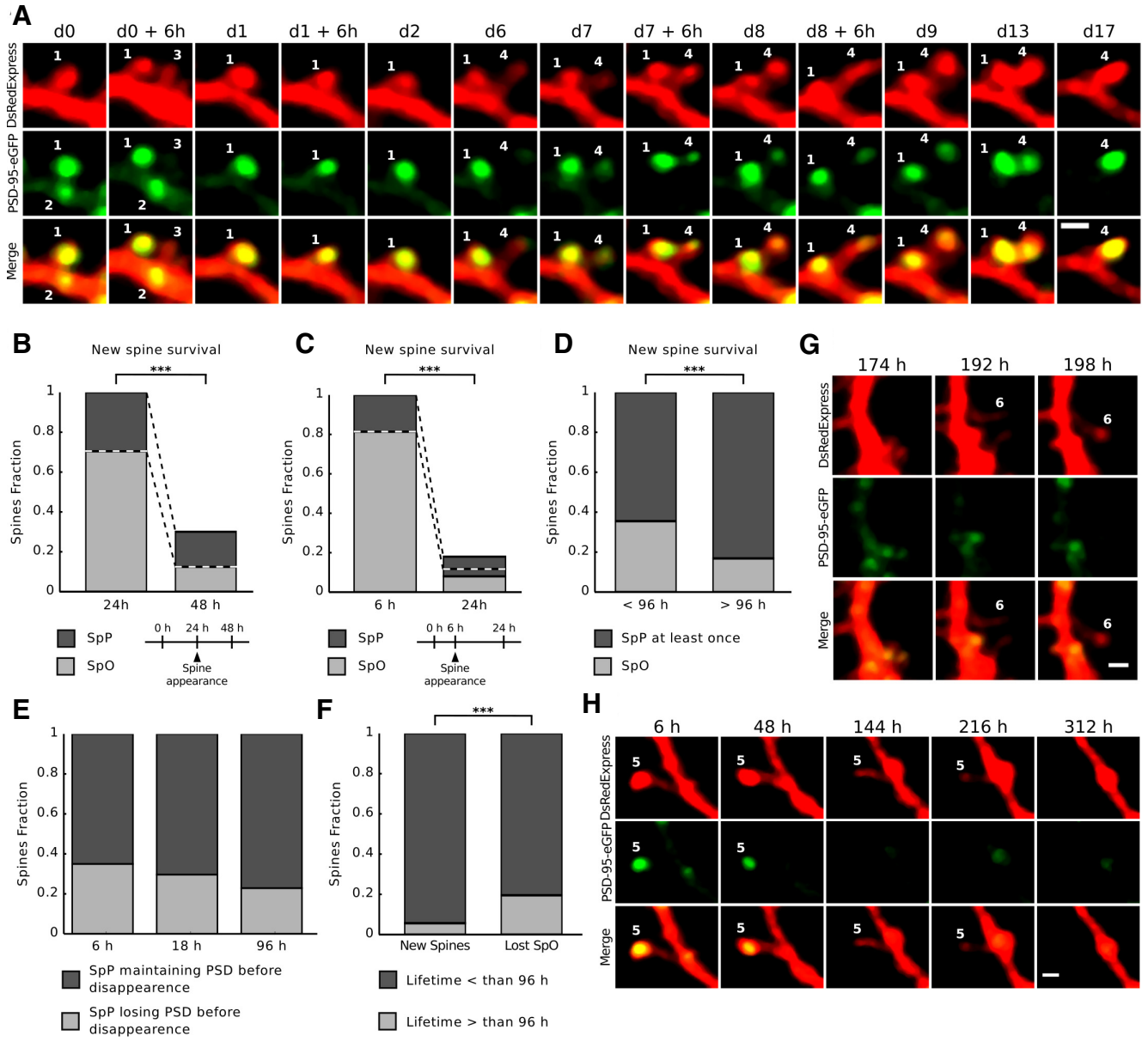


**Figure 5.** ***A***, Time-lapse image of a dendritic region containing the following: a SpP disappearing after day 13 (#1); a PO disappearing after the second imaging session on day 0 (#2); a transient SpO appearing and disappearing within 24 h after the first imaging session (#3); and a new spine appearing as a SpO on day 6 and turning into a SpP on day 7 (#4). Scale bar, 1 $\mu$m. ***B***, Fraction of new spines (<24 h old) that survives over the next 24 h. The fraction of new SpPs that is still present after 24 h is larger than the fraction of SpOs (***$p < 0.005$). ***C***, Fraction of new spines (<6 h old) that survives over the next 18 h. The fraction of new SpPs that is still present after 18 h is larger than the fraction of SpOs (***$p < 0.005$). ***D***, New spines that show a PSD-95-eGFP punctum at least once during their lifetime have a higher probability of surviving for >96 h (***$p < 0.005$). ***E***, Fractions of lost SpPs that maintain or lose their PSD-95-eGFP punctum before disappearance. ***F***, Left, Fraction of new SpOs with lifetimes of more or <96 h. Right, Fraction of SpPs that continue as SpOs for more or <96 h before disappearing (***$p < 0.005$). ***G***, New SpO that is present over two time points (#6). Scale bar, 1 $\mu$m. ***H***, Disappearing spine that loses its PSD-95-eGFP punctum before pruning (#5). Scale bar, 1 $\mu$m.

To investigate the interaction between the presence of PSD-95-eGFP puncta and spine loss, we selected a population of SpPs that were present on the first imaging time point ($t = 0$ h) yet were lost over the course of the experiment (after $t = 6$ h). The lost spines were grouped into three categories: those last seen before an interval of 6, 18, and 96 h. Although the majority of spines that disappeared still had a PSD-95-eGFP punctum on the last time point (6 h, 65%; Fig. 5*E*), a substantial fraction had lost their puncta before their disappearance (6 h, 35%; Fig. 5*H*, #5). The fraction of spines that had lost their PSD-95-eGFP punctum before their disappearance tended to decrease gradually with an increase of the interval time, but we did not detect a significant difference (Fig. 5*E*). This suggests that, in general, spine and synapse disappearance happens concomitantly (over the course of hours). However, some spines may persist for some time, even after they have lost their PSD (Fig. 5*H*). A total of 20% of the disappearing spines survived for >96 h after they had lost their PSD-95-eGFP punctum (Fig. 5*F*). This fraction is significantly higher compared with new spines that never accumulate a PSD-95-eGFP punctum (5%, $p < 0.005$ $\chi^2$; Fig. 5*F*). This suggests that, once spines have acquired a PSD, their survival rate increases even when they lose their synapse.

### Spine volume and PSD-95 size are linearly related

EM studies have indicated that spine and synapse size are positively correlated (Harris and Stevens, 1989; Nusser et al., 1998;

Takumi et al., 1999; Holtmaat et al., 2005; Knott et al., 2006). Electrophysiology and imaging studies *in vitro* have confirmed this finding (Matsuzaki et al., 2001; Zito et al., 2004). The FIBSEM reconstructions show that PSD size is proportional to the brightness of PSD-95-eGFP in spines (Fig. 3*C*). This suggests that spine brightness *in vivo* is proportional to PSD-95-eGFP brightness. In general, we observed that bright spines in the red channel also contained high green fluorescence intensity levels (Figs. 5*A*, 6*A*). Conversely, dim spines in the red channel contained low green fluorescence intensities. To investigate quantitatively the relationship between spine size and putative PSD size, we selected a random population of SpPs ($n = 108$) that were seen on the first imaging session. It was shown previously that spine brightness, as measured in single 2PLSM optical sections, is monotonically related to spine volume (Holtmaat et al., 2005; Mostany et al., 2013). Here, we assumed that the brightness of PSD-95-eGFP reliably represents the PSD size. Because the absolute fluorescence levels differed between animals and different cells, we normalized the integrated red and green fluorescence intensity in the spine head to the mean of the maximum pixel values that we encountered in a 1 to 3 $\mu$m stretch of parent dendrite just below the spine (Fig. 6*B*). Both green and red fluorescence intensities in spines followed a log-normal distribution (data not shown; Loewenstein et al., 2011). A regression analysis revealed a linear relationship between red and green intensities in the spine head ($R^2 = 0.79$, $r = 7.12$; Fig. 6*C*). These data corroborate previous EM studies (Harris and Stevens, 1989; Knott et al., 2006) and indicate that the expression of PSD-95-eGFP does not disturb the relationship between spine and PSD size.

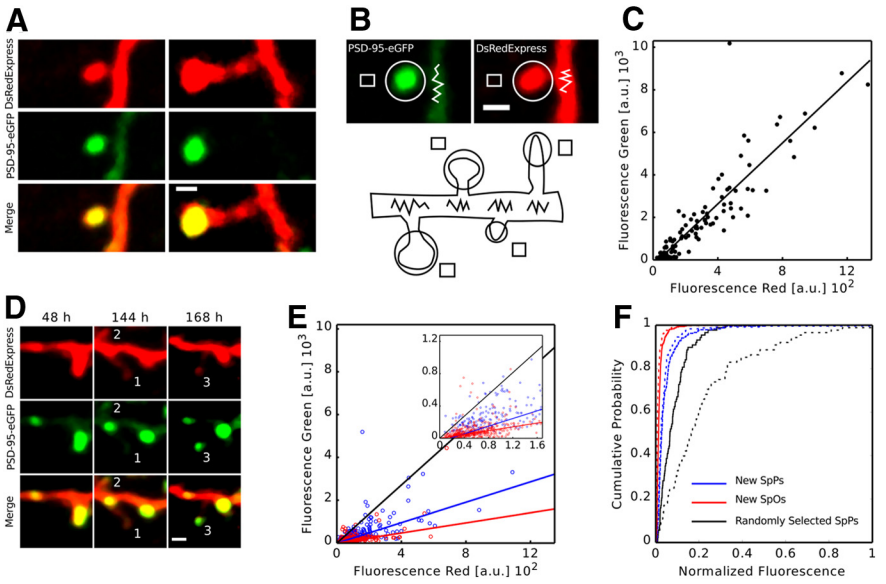


**Figure 6.** ***A***, Examples of SpPs with small (left) and large (right) volumes. ***B***, Procedure for measurement of DsRedExpress and PSD-95-eGFP fluorescence intensities. In brightest optical section of each channel, background-corrected pixel intensities are integrated over an area spanning the spine head (circles). Background pixel values are taken from nearby regions (rectangles). In each region of interest, spine values are normalized to the average maximum pixel values of neighboring areas in the dendritic shaft (jagged lines). ***C***, Linear correlation between green and red fluorescence intensities in a random set of SpPs at $t = 0$ h. ***D***, New SpO (#1) and a new SpPs (#2 and #3). ***E***, Linear fits of red and green fluorescence for new SpPs (blue), new SpOs (red), and spines from ***C*** (black). Inset shows the smallest data points. ***F***, Cumulative distribution of red (continuous lines) and green (dotted lines) fluorescence intensities for all spines from ***E*** and ***C***. Scale bars, 1 $\mu$m.

### Relationship between spine formation and PSD size

To investigate the interaction between PSD size and new spine formation, we measured the levels of PSD-95-eGFP and new spine volumes. We selected a random population of new spines that had appeared at any time point and analyzed their normalized spine head volume and PSD sizes on the first time point of observation (Fig. 6*D*,*E*). The population of new spines was divided into those that were classified as SpP (Fig. 6*D*, #2 and #3; Fig. 6*E*, blue dots) and SpO (Fig. 5*D*, #1; Fig. 6*E*, red dots). As expected, in the SpO subpopulation, the PSD-95-eGFP intensity modestly increased with spine volume. In new SpPs, the slope of the interaction was steeper ($r_{SpP} = 2.38$, range 2.31–2.46; $r_{SpO} = 1.18$, range 1.14–1.22; robust regression analysis), but still shallower than for randomly selected SpPs. Therefore, the cytosolic volumes and the PSD-95-eGFP levels of new spines that had acquired a PSD were significantly larger than the volumes of new spines without a PSD and their respective normalized cumulative distributions were significantly different (Fig. 6*F*; dotted lines vs dotted lines, $p < 0.005$; solid lines vs solid lines, $p < 0.005$; KS test). These data indicate that, on average, young new spines contain smaller PSDs relative to their head volume compared with persistent spines. This may be indicative of a synaptic maturation process that lags spine enlargement.

### PSD size changes correlate with spine volume changes

Spine head volumes have been shown to fluctuate *in vivo*, even in persistent spines (Holtmaat et al., 2005; Holtmaat et al., 2006; Hofer et al., 2009; Loewenstein et al., 2011). Although spine volume and synapse size are tightly coupled, it could not be deduced from these experiments whether PSD sizes closely follow spine volume changes. We estimated spine head volume and PSD size alterations of persistent spines by measuring the ratio of fluorescence intensities between two consecutive time points (intervals of 6, 18, and 96 h) in both the green and red channel. This analysis confirmed that spine head volumes fluctuate continuously. PSD size changes and spine head volume changes could be fit with a linear function ($r = 0.6$; $n = 1224$; Fig. 6*A*), but the correlation between the magnitudes of the changes was poor ($R^2 = 0.26$). In a small fraction (162 of 1224, 13.2%) of sampled spines, the PSD size and spine head volume dynamics were anisometric; that is, the spine grew whereas the PSD shrunk or vice versa (Fig. 7*A*, quadrant II and IV). These types may represent spines that had undergone synaptic weakening or strengthening shortly before they were imaged, because the initial phase (5–10 min) of long-term potentiation (LTP) induction shows relatively poor interactions between spine head size and synapse strength (Matsuzaki et al., 2004; Lee et al., 2009).

To investigate the relationship between spine stability and PSD size and spine head volume changes, we compared the changes over two time points for new spines and lost spines with persistent spines (Fig. 7*B*). A random set of new SpPs was selected at various time points (from $t = 6$ h onward) and their size was measured on the first and second time point on which they were detected (Fig. 7*D*). Lost spines were defined as those that were detected with a PSD-95-eGFP punctum on the first imaging day

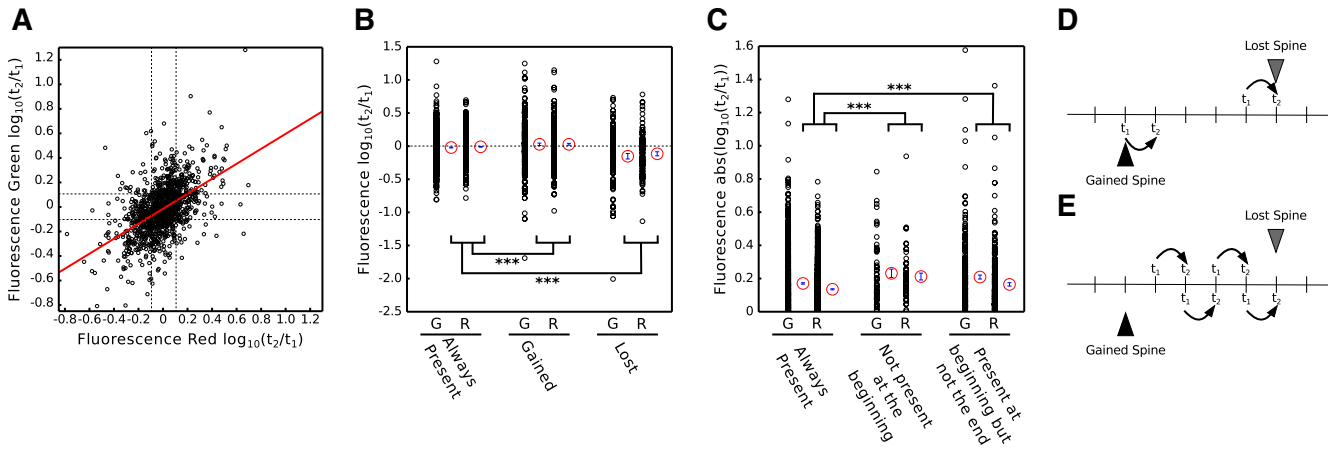


**Figure 7.** ***A***, Relationship between changes in red and green fluorescence intensities. Dotted lines represent the measurement error. ***B***, New spines display an increase in both green and red fluorescence over the first two time points after their appearance compared with persistent spines (***$p < 0.005$). Lost spines display a decrease in both green and red fluorescence over the last two time points before their disappearance compared with persistent spines (***$p < 0.005$). ***C***, Absolute value of fluorescence intensity ratios over a random set of two consecutive time points for persistent, new, and preexisting disappearing spines. New and lost spines display increased fluctuations (***$p < 0.005$). ***D***, Example of a time interval used in ***B***. ***E***, Example of time intervals used in ***C***.

($t = 0$ h) and were subsequently lost over the time course of the experiment. Their sizes were measured on the last two time points at which they were detected. Despite numerous large fluctuations (e.g., >3-fold changes), on average, growth and shrinkage canceled out one another in persistent spines (PSD-95-eGFP, $-0.048 \pm 0.015$; DsRedExpress, $-0.023 \pm 0.013$, $n = 1224$; Fig. 7*B*). This may be indicative of homeostatic processes that keep synapse strength, and thereby PSD size, equal over time (Turrigiano and Nelson, 2004). Conversely, the $\log_{10}$ ratios were slightly skewed toward positive values for new spines and toward negative values for lost spines (new: PSD-95-eGFP, $0.064 \pm 0.042$; DsRedExpress, $0.065 \pm 0.033$; $n = 386$, $p < 0.005$, *t* test between persistent and new; lost: PSD-95-eGFP, $-0.366 \pm 0.093$; DsRedExpress, $-0.298 \pm 0.068$; $n = 117$, $p < 0.005$, *t* test between persistent and lost). To determine whether those types of spines displayed different structural dynamics over their whole lifetime, we measured fluorescence changes in a randomly selected set of imaging time points and intervals (Fig. 7*E*) and took the absolute value of the ratios between the two time points to assess the variance in the changes. New and lost spines displayed increased PSD size and spine head volume fluctuations, indicating that their synapses are generally less stable than those of persistent spines (persistent: PSD-95-eGFP, $0.393 \pm 0.010$; DsRedExpress, $0.311 \pm 0.008$, $n = 1224$; new: PSD-95-eGFP, $0.533 \pm 0.058$; DsRedExpress, $0.488 \pm 0.047$; $n = 37$, $p < 0.005$, *t* test; lost: PSD-95-eGFP, $0.481 \pm 0.027$; DsRedExpress, $0.379 \pm 0.024$; $n = 277$, $p < 0.005$, *t* test; Fig. 7*C*). The increased PSD dynamics may be a signature of spines that are still in a growth process or are destined to disappear.

## Discussion

We have characterized the relationship between PSD dynamics and spine stability in real time *in vivo*. Our data show that the expression of PSD-95-eGFP *in vivo* allows the identification of the smallest PSDs seen in EM (Fig. 3). Persistent spines almost always bear a PSD (Figs. 4, 5). Two-thirds of the new spines and spines that are destined to be lost lack a clear PSD (Figs. 4, 5). New spines that acquire a PSD are more likely to become persistent (Fig. 5). However, most PSD-bearing new spines are transient. Persistent spines that lose a PSD are likely to be pruned (Fig. 5). Furthermore, PSD size is proportional to spine head volume (Fig. 6). The PSD to head size ratio of new spines is lower than in persistent spines, suggesting that they slowly increase their PSD content. Spines that are destined to be lost on average lose PSD content over hours to days before they are pruned (Fig. 7).

### Auxiliary expression of PSD-95 and scoring of PSD-95-eGFP puncta

PSD-95 overexpression has been shown to increase LTP-like plasticity and synapse maturation in neuronal cultures and organotypic brain slices (El-Husseini et al., 2000; Ehrlich and Malinow, 2004; Ehrlich et al., 2007). Therefore, in our study, the auxiliary expression of PSD-95 may have altered synaptic physiology. However, several observations indicate that the disturbing effects were minimal. We expressed PSD-95-eGFP in a similar way to Gray et al. (2006), in which spine densities and synaptic connectivity were not affected. Spine densities were similar to other *in vivo* imaging studies (Holtmaat et al., 2005; Gray et al., 2006; Hofer et al., 2009), and spine turnover rates were comparable to those in GFP-transgenic mice (Holtmaat et al., 2005; Wilbrecht et al., 2010). Furthermore, spine sizes and PSD sizes followed a log-normal distribution, similar to a recent imaging study *in vivo* (Loewenstein et al., 2011), and individual spines and PSDs alternately grew and shrunk over time. Many new spines never acquired PSDs or only expressed them transiently. Many previously persistent spines lost their PSDs before being pruned. Altogether, this confirms that the auxiliary expression of PSD-95 did not cause a continuous growth of PSDs, did not massively stabilize spines, and still allowed continuous spine and synapse pruning. This also suggests that the synaptic incorporation of PSD-95 is a regulated process that is not readily inflated by auxiliary expression, which holds true for various other synaptic proteins (Kessels et al., 2009).

In our study, the number of spines without a PSD was comparable but slightly higher compared with some *in vitro* (De Roo et al., 2008) and EM studies (Knott et al., 2006; Arellano et al., 2007). Spine characteristics vary between cell and dendrite types (Nimchinsky et al., 2002). Therefore, a likely explanation is the difference in neuron and dendrite populations that were analyzed in those studies. We are confident that our scoring criteria detected the smallest PSDs. The results were similar when we based scoring criteria on a cluster analysis of the fraction of PSD-95-

eGFP that was bound in spine heads (Otmakhov et al., 2004). Furthermore, the EM reconstruction showed that the lowest fluorescence intensities that we classified as puncta corresponded to the smallest PSDs that can be seen at the ultrastructural level. In addition, it should also be noted that a large proportion of the spine population without a PSD represented very thin structures, which may often be overlooked in serial section EM. For example, the widths of some thin spines in our 2PLSM images that were reconstructed using FIBSEM were as little as 80 nm. These could have remained undetected without the information from the live imaging that indicated their presence.

### Relationship between spine and PSD formation

The majority of gained spines did not stabilize and did not acquire a distinct PSD. This corroborates EM studies that have detected a lack of PSDs and/or synapses in a large fraction of newly formed spines (Knott et al., 2006; Nägerl et al., 2007). New SpOs rarely acquired a PSD later on. However, we also observed an increasing fraction of new SpPs with increasing time intervals. This indicates that PSD-95 clustering is not always immediate, but can occur over hours and days after the growth of the parent spine. PSD growth showed similarities to *in vitro* studies. However, they were quantitatively different from the fast and functional synapse formation seen in those experiments (Nägerl et al., 2007; Zito et al., 2009). There are several explanations. First, our PSD scoring criteria may have resulted in a slight underestimation of synapse formation (see Results). Second, synaptic-like activity may occur even when PSDs are small or absent through nonclustered NMDA and AMPA receptors that are juxtaposed to presynaptic boutons. Third, PSD formation may be slower *in vivo* compared with organotypic cultures. This could be due to differences in circuit activity, synaptic inhibition, and neuromodulation. In our experiments, the dendrites were positioned in L1, a region of the cortex that receives many modulatory and long-range connections, whereas most slice experiments focused on hippocampal pyramidal cells that lacked long-range modulatory inputs and hormonal regulation. Hormonal oscillations and modulatory inputs can have profound effects on synaptic plasticity and spine maturation (Jones et al., 2009; Liston et al., 2013).

Some new spines displayed a PSD yet did not stabilize for long periods of time. However, they still persisted longer than spines without PSDs. This suggests that, in addition to the PSD, other factors determine the stabilization of the spine. This is not inconceivable because spine morphology is regulated through a vast signaling network (Patterson and Yasuda, 2011). Because we did not have insight into axonal bouton dynamics, we can also not exclude the possibility that some PSDs lacked a presynaptic counterpart. Spine and PSD formation might be induced by large quantities of presynaptic glutamate release or spillover (Richards et al., 2005; Kwon and Sabatini, 2011). However, these spines may not always be able to contact the presynaptic site from which glutamate was released. Alternatively, synapses in those spines may not be potentiated and therefore fail to stabilize, which may cause the spines to retract (Matsuzaki et al., 2004; Kopec et al., 2006; Harvey and Svoboda, 2007; Hill and Zito, 2013; Oh et al., 2013). Nevertheless, our data imply that transient SpPs may serve to provide short-term synaptic connections and could thereby temporarily influence network activity. This may be important for learning and downstream neuronal network plasticity (Xu et al., 2009; Yang et al., 2009).

### Relationship between spine loss and PSD dynamics

PSD-95-eGFP levels in persistent spines fluctuated. We found a concomitant decrease in spine volume and PSD-95-eGFP levels before spines were pruned. This indicates that spine loss is associated with a gradual loss of PSD components. A gradual reduction of spine volumes before spine pruning was also observed during the experience dependent loss of persistent spines (Holtmaat et al., 2006). These observations fit well with intrinsic spine volume changes in organotypic brain slices (Yasumatsu et al., 2008) and multiplicative dynamics *in vivo* (Loewenstein et al., 2011). The results may indicate that the maintenance of a spine relies on PSD size. New spines that do not acquire enough PSD molecules may disappear and old spines that lose too many may be pruned. The loss of PSD components likely depends on long-term depression (Nägerl et al., 2004; Zhou et al., 2004; Oh et al., 2013). Synaptic adhesion molecules that are linked to PSDs may be key in the maintenance of a synapse (Sheng and Hoogenraad, 2007; Han and Kim, 2008). Once the PSD size is reduced below a critical point, adhesion to the presynaptic bouton may become insufficient to maintain the synaptic connection. Spines without a synapse may spontaneously disappear due to a lack of filamentous actin-anchoring points (Sekino et al., 2007; Soria Fregozo and Perez Vega, 2012). Conversely, we did observe persistent spines that temporarily existed without a PSD before being lost (Fig. 5*H*). We cannot exclude the possibility that, in some cases, the spine was lost and replaced by a new spine that had not (yet) acquired a PSD. Nonetheless, the result may indicate that some, perhaps nonsynaptic, adhesion molecules temporarily keep the spine head linked to the presynaptic bouton after the complete removal of the PSD.

Similar to Woods et al. (2011), we found that the loss of PSD enrichment is not a prerequisite for spine loss. Many spines displayed normal PSD-95-GFP levels at the last time point of observation. This may indicate that spines can be very rapidly pruned after the loss of a synapse. An interesting alternative is that active spine pruning in some cases strips the synaptic contact, a process that could be modulated by nonsynaptic mechanisms. However, it should be noted that most of our time intervals were much longer than in the *in vitro* studies and we may not have captured rapid PSD decline before spine pruning.

## References

Arellano JI, Espinosa A, Fairén A, Yuste R, DeFelipe J (2007) Non-synaptic dendritic spines in neocortex. Neuroscience 145:464–469. CrossRef Medline

Cardona A, Saalfeld S, Schindelin J, Arganda-Carreras I, Preibisch S, Longair M, Tomancak P, Hartenstein V, Douglas RJ (2012) TrakEM2 software for neural circuit reconstruction. PLoS One 7:e38011. CrossRef Medline

Chen X, Vinade L, Leapman RD, Petersen JD, Nakagawa T, Phillips TM, Sheng M, Reese TS (2005) Mass of the postsynaptic density and enumeration of three key molecules. Proc Natl Acad Sci U S A 102:11551–11556. CrossRef Medline

Chen X, Nelson CD, Li X, Winters CA, Azzam R, Sousa AA, Leapman RD, Gainer H, Sheng M, Reese TS (2011) PSD-95 is required to sustain the molecular organization of the postsynaptic density. J Neurosci 31:6329–6338. CrossRef Medline

Craven SE, El-Husseini AE, Bredt DS (1999) Synaptic targeting of the postsynaptic density protein PSD-95 mediated by lipid and protein motifs. Neuron 22:497–509. CrossRef Medline

De Roo M, Klauser P, Mendez P, Poglia L, Muller D (2008) Activity-dependent PSD formation and stabilization of newly formed spines in hippocampal slice cultures. Cereb Cortex 18:151–161. CrossRef Medline

Ehrlich I, Malinow R (2004) Postsynaptic density 95 controls AMPA receptor incorporation during long-term potentiation and experience-driven synaptic plasticity. J Neurosci 24:916–927. Medline

Ehrlich I, Klein M, Rumpel S, Malinow R (2007) PSD-95 is required for

activity-driven synapse stabilization. Proc Natl Acad Sci U S A 104:4176–4181. CrossRef Medline

El-Husseini AE, Schnell E, Chetkovich DM, Nicoll RA, Bredt DS (2000) PSD-95 involvement in maturation of excitatory synapses. Science 290:1364–1368. CrossRef Medline

Fu M, Zuo Y (2011) Experience-dependent structural plasticity in the cortex. Trends Neurosci 34:177–187. CrossRef Medline

Gray NW, Weimer RM, Bureau I, Svoboda K (2006) Rapid redistribution of synaptic PSD-95 in the neocortex in vivo. PLoS Biol 4:e370. CrossRef Medline

Grillo FW, Song S, Teles-Grilo Ruivo LM, Huang L, Gao G, Knott GW, Maco B, Ferretti V, Thompson D, Little GE, De Paola V (2013) Increased axonal bouton dynamics in the aging mouse cortex. Proc Natl Acad Sci U S A 110:E1514–1523. CrossRef Medline

Han K, Kim E (2008) Synaptic adhesion molecules and PSD-95. Progress in neurobiology 84:263–283. CrossRef Medline

Harris KM, Stevens JK (1989) Dendritic spines of CA1 pyramidal cells in the rat hippocampus: serial electron microscopy with reference to their biophysical characterisitcs. J Neurosci 9:2982–2997. Medline

Harvey CD, Svoboda K (2007) Locally dynamic synaptic learning rules in pyramidal neuron dendrites. Nature 450:1195–1200. CrossRef Medline

Hill TC, Zito K (2013) LTP-induced long-term stabilization of individual nascent dendritic spines. J Neurosci 33:678–686. CrossRef Medline

Hofer SB, Mrsic-Flogel TD, Bonhoeffer T, Hübener M (2009) Experience leaves a lasting structural trace in cortical circuits. Nature 457:313–317. CrossRef Medline

Holtmaat A, Svoboda K (2009) Experience-dependent structural synaptic plasticity in the mammalian brain. Nat Rev Neurosci 10:647–658. CrossRef Medline

Holtmaat AJ, Trachtenberg JT, Wilbrecht L, Shepherd GM, Zhang X, Knott GW, Svoboda K (2005) Transient and persistent dendritic spines in the neocortex in vivo. Neuron 45:279–291. CrossRef Medline

Holtmaat A, Wilbrecht L, Knott GW, Welker E, Svoboda K (2006) Experience-dependent and cell-type-specific spine growth in the neocortex. Nature 441:979–983. CrossRef Medline

Holtmaat A, Bonhoeffer T, Chow DK, Chuckowree J, De Paola V, Hofer SB, Hübener M, Keck T, Knott G, Lee WC, Mostany R, Mrsic-Flogel TD, Nedivi E, Portera-Cailliau C, Svoboda K, Trachtenberg JT, Wilbrecht L (2009) Long-term, high-resolution imaging in the mouse neocortex through a chronic cranial window. Nat Protoc 4:1128–1144. CrossRef Medline

Jones KA, Srivastava DP, Allen JA, Strachan RT, Roth BL, Penzes P (2009) Rapid modulation of spine morphology by the 5-HT2A serotonin receptor through kalirin-7 signaling. Proc Natl Acad Sci U S A 106:19575–19580. CrossRef Medline

Judkewitz B, Rizzi M, Kitamura K, Häusser M (2009) Targeted single-cell electroporation of mammalian neurons in vivo. Nat Protoc 4:862–869. CrossRef Medline

Kelsch W, Lin CW, Lois C (2008) Sequential development of synapses in dendritic domains during adult neurogenesis. Proc Natl Acad Sci U S A 105:16803–16808. CrossRef Medline

Kessels HW, Kopec CD, Klein ME, Malinow R (2009) Roles of stargazin and phosphorylation in the control of AMPA receptor subcellular distribution. Nat Neurosci 12:888–896. CrossRef Medline

Knott GW, Holtmaat A, Wilbrecht L, Welker E, Svoboda K (2006) Spine growth precedes synapse formation in the adult neocortex in vivo. Nat Neurosci 9:1117–1124. CrossRef Medline

Kopec CD, Li B, Wei W, Boehm J, Malinow R (2006) Glutamate receptor exocytosis and spine enlargement during chemically induced long-term potentiation. J Neurosci 26:2000–2009. CrossRef Medline

Kwon HB, Sabatini BL (2011) Glutamate induces de novo growth of functional spines in developing cortex. Nature 474:100–104. CrossRef Medline

Lee SJ, Escobedo-Lozoya Y, Szatmari EM, Yasuda R (2009) Activation of CaMKII in single dendritic spines during long-term potentiation. Nature 458:299–304. CrossRef Medline

Liston C, Cichon JM, Jeanneteau F, Jia Z, Chao MV, Gan WB (2013) Circadian glucocorticoid oscillations promote learning-dependent synapse formation and maintenance. Nat Neurosci 16:698–705. CrossRef Medline

Livneh Y, Feinstein N, Klein M, Mizrahi A (2009) Sensory input enhances synaptogenesis of adult-born neurons. J Neurosci 29:86–97. CrossRef Medline

Loewenstein Y, Kuras A, Rumpel S (2011) Multiplicative dynamics underlie the emergence of the log-normal distribution of spine sizes in the neocortex in vivo. J Neurosci 31:9481–9488. CrossRef Medline

Maco B, Holtmaat A, Cantoni M, Kreshuk A, Straehle CN, Hamprecht FA, Knott GW (2013) Correlative in vivo 2 photon and focused ion beam scanning electron microscopy of cortical neurons. PloS One 8:e57405. CrossRef Medline

Matsuzaki M, Ellis-Davies GC, Nemoto T, Miyashita Y, Iino M, Kasai H (2001) Dendritic spine geometry is critical for AMPA receptor expression in hippocampal CA1 pyramidal neurons. Nat Neurosci 4:1086–1092. CrossRef Medline

Matsuzaki M, Honkura N, Ellis-Davies GC, Kasai H (2004) Structural basis of long-term potentiation in single dendritic spines. Nature 429:761–766. CrossRef Medline

Mostany R, Anstey JE, Crump KL, Maco B, Knott G, Portera-Cailliau C (2013) Altered synaptic dynamics during normal brain aging. J Neurosci 33:4094–4104. CrossRef Medline

Nägerl UV, Eberhorn N, Cambridge SB, Bonhoeffer T (2004) Bidirectional activity-dependent morphological plasticity in hippocampal neurons. Neuron 44:759–767. CrossRef Medline

Nägerl UV, Köstinger G, Anderson JC, Martin KA, Bonhoeffer T (2007) Protracted synaptogenesis after activity-dependent spinogenesis in hippocampal neurons. J Neurosci 27:8149–8156. CrossRef Medline

Niell CM, Meyer MP, Smith SJ (2004) In vivo imaging of synapse formation on a growing dendritic arbor. Nat Neurosci 7:254–260. CrossRef Medline

Nimchinsky EA, Sabatini BL, Svoboda K (2002) Structure and function of dendritic spines. Annu Rev Physiol 64:313–353. CrossRef Medline

Nusser Z, Lujan R, Laube G, Roberts JD, Molnar E, Somogyi P (1998) Cell type and pathway dependence of synaptic AMPA receptor number and variability in the hippocampus. Neuron 21:545–559. CrossRef Medline

Oh WC, Hill TC, Zito K (2013) Synapse-specific and size-dependent mechanisms of spine structural plasticity accompanying synaptic weakening. Proc Natl Acad Sci U S A 110:E305–312. CrossRef Medline

Okabe S, Kim HD, Miwa A, Kuriu T, Okado H (1999) Continual remodeling of postsynaptic density and its regulation by synaptic activity. Nat Neurosci 2:804–811. CrossRef Medline

Okabe S, Miwa A, Okado H (2001) Spine formation and correlated assembly of presynaptic and postsynaptic molecules. J Neurosci 21:6105–6114. Medline

Otmakhov N, Tao-Cheng JH, Carpenter S, Asrican B, Dosemeci A, Reese TS, Lisman J (2004) Persistent accumulation of calcium/calmodulin-dependent protein kinase II in dendritic spines after induction of NMDA receptor-dependent chemical long-term potentiation. J Neurosci 24:9324–9331. Medline

Patterson M, Yasuda R (2011) Signalling pathways underlying structural plasticity of dendritic spines. Br J Pharmacol 163:1626–1638. CrossRef Medline

Pologruto TA, Sabatini BL, Svoboda K (2003) ScanImage: Flexible software for operating laser-scanning microscopes. BioMedical Engineering OnLine 2:13. Medline

Prange O, Murphy TH (2001) Modular transport of postsynaptic density-95 clusters and association with stable spine precursors during early development of cortical neurons. J Neurosci 21:9325–9333. Medline

Richards DA, Mateos JM, Hugel S, de Paola V, Caroni P, Gähwiler BH, McKinney RA (2005) Glutamate induces the rapid formation of spine head protrusions in hippocampal slice cultures. Proc Natl Acad Sci U S A 102:6166–6171. CrossRef Medline

Saito T, Nakatsuji N (2001) Efficient gene transfer into the embryonic mouse brain using in vivo electroporation. Dev Biol 240:237–246. CrossRef Medline

Sala C, Futai K, Yamamoto K, Worley PF, Hayashi Y, Sheng M (2003) Inhibition of dendritic spine morphogenesis and synaptic transmission by activity-inducible protein Homer1a. J Neurosci 23:6327–6337. Medline

Sekino Y, Kojima N, Shirao T (2007) Role of actin cytoskeleton in dendritic spine morphogenesis. Neurochem Int 51:92–104. CrossRef Medline

Sharma K, Fong DK, Craig AM (2006) Postsynaptic protein mobility in

dendritic spines: long-term regulation by synaptic NMDA receptor activation. Mol Cell Neurosci 31:702–712. CrossRef Medline

Sheng M, Hoogenraad CC (2007) The postsynaptic architecture of excitatory synapses: a more quantitative view. Annu Rev Biochem 76:823–847. CrossRef Medline

Soria Fregozo C, Pérez Vega MI (2012) Actin-binding proteins and signalling pathways associated with the formation and maintenance of dendritic spines. Neurologia 27:421–431. Medline

Tabata H, Nakajima K (2001) Efficient in utero gene transfer system to the developing mouse brain using electroporation: visualization of neuronal migration in the developing cortex. Neuroscience 103:865–872. CrossRef Medline

Takumi Y, Ramírez-León V, Laake P, Rinvik E, Ottersen OP (1999) Different modes of expression of AMPA and NMDA receptors in hippocampal synapses. Nat Neurosci 2:618–624. CrossRef Medline

Turrigiano GG, Nelson SB (2004) Homeostatic plasticity in the developing nervous system. Nat Rev Neurosci 5:97–107. CrossRef Medline

Wilbrecht L, Holtmaat A, Wright N, Fox K, Svoboda K (2010) Structural plasticity underlies experience-dependent functional plasticity of cortical circuits. J Neurosci 30:4927–4932. CrossRef Medline

Woods GF, Oh WC, Boudewyn LC, Mikula SK, Zito K (2011) Loss of PSD-95 enrichment is not a prerequisite for spine retraction. J Neurosci 31:12129–12138. CrossRef Medline

Xu T, Yu X, Perlik AJ, Tobin WF, Zweig JA, Tennant K, Jones T, Zuo Y (2009) Rapid formation and selective stabilization of synapses for enduring motor memories. Nature 462:915–919. CrossRef Medline

Yang G, Pan F, Gan WB (2009) Stably maintained dendritic spines are associated with lifelong memories. Nature 462:920–924. CrossRef Medline

Yasumatsu N, Matsuzaki M, Miyazaki T, Noguchi J, Kasai H (2008) Principles of long-term dynamics of dendritic spines. J Neurosci 28:13592–13608. CrossRef Medline

Zhou Q, Homma KJ, Poo MM (2004) Shrinkage of dendritic spines associated with long-term depression of hippocampal synapses. Neuron 44:749–757. CrossRef Medline

Zito K, Knott G, Shepherd GM, Shenolikar S, Svoboda K (2004) Induction of spine growth and synapse formation by regulation of the spine actin cytoskeleton. Neuron 44:321–334. CrossRef Medline

Zito K, Scheuss V, Knott G, Hill T, Svoboda K (2009) Rapid functional maturation of nascent dendritic spines. Neuron 61:247–258. CrossRef Medline

Zuo Y, Lin A, Chang P, Gan WB (2005) Development of long-term dendritic spine stability in diverse regions of cerebral cortex. Neuron 46:181–189. CrossRef Medline